Atmos. Chem. Phys. Discuss., 12, 20073–20111, 2012
www.atmos-chem-phys-discuss.net/12/20073/2012/
doi:10.5194/acpd-12-20073-2012

Atmospheric Chemistry and Physics Discussions

Estimates of aerosol radiative forcing from the MACC re-analysis

N. Bellouin[1], J. Quaas[2], J.-J. Morcrette[3], and O. Boucher[4]

[1]Met Office Hadley Centre, Exeter, UK
[2]Universität Leipzig, Leipzig, Germany
[3]European Centre for Medium-range Weather Forecast, Reading, UK
[4]Laboratoire de Météorologie Dynamique, IPSL, CNRS/UPMC, Paris, France

Received: 26 July 2012 – Accepted: 3 August 2012 – Published: 10 August 2012

Correspondence to: N. Bellouin (nicolas.bellouin@metoffice.gov.uk)

Published by Copernicus Publications on behalf of the European Geosciences Union.

Abstract

The European Centre for Medium-range Weather Forecast (ECMWF) provides an aerosol re-analysis starting from year 2003 for the Monitoring Atmospheric Composition and Climate (MACC) project. The re-analysis assimilates total aerosol optical depth retrieved by the Moderate Resolution Imaging Spectroradiometer (MODIS) to correct for model departures from observed aerosols. The re-analysis therefore combines satellite retrievals with the full spatial coverage of a numerical model. Re-analysed products are used here to estimate the shortwave direct and first indirect radiative forcing of anthropogenic aerosols over the period 2003–2010, using methods previously applied to satellite retrievals of aerosols and clouds. The best estimate of globally-averaged, all-sky direct radiative forcing is $-0.5\,\mathrm{Wm}^{-2}$. Accounting for uncertainties in the aerosol anthropogenic fraction, aerosol absorption, and cloudy-sky effects, results in the direct radiative forcing being bounded by -0.8 and $0\,\mathrm{Wm}^{-2}$. Further accounting for differences between the present-day natural and pre-industrial aerosols provides a direct radiative forcing estimate in the range -0.5 to $0\,\mathrm{Wm}^{-2}$, with a best estimate of $-0.3\,\mathrm{Wm}^{-2}$. The best estimate of globally-averaged, all-sky first indirect radiative forcing is $-0.4\,\mathrm{Wm}^{-2}$. Accounting for uncertainties in the aerosol anthropogenic fraction, cloud albedo, and cloud droplet number concentration susceptibility to aerosol changes, lower and upper bounds of the first indirect radiative forcing are $-2.1\,\mathrm{Wm}^{-2}$ and $-0.1\,\mathrm{Wm}^{-2}$. In order to decrease uncertainty ranges, better observational constraints on aerosol absorption and susceptibility of cloud droplet number concentrations to aerosol changes are required.

1 Introduction

The main interactions between natural and anthropogenic aerosols and the climate system are through scattering and absorption of radiation (direct radiative effect, DRE), and modification of the microphysical properties of clouds, impacting cloud albedo (first

ACPD
12, 20073–20111, 2012

indirect effect), cloud evolution and precipitation efficiency (second indirect effect). Anthropogenic aerosols, emitted into the atmosphere by human activities, are considered external to the climate system, and their marginal contributions to the direct and indirect effects are termed forcing (Forster et al., 2007).

Direct and first indirect radiative forcing, hereafter abbreviated as DRF and IRF, respectively, have been estimated using aerosol numerical modelling or satellite retrievals. Numerical models simulate the complexity of real aerosol distributions, but make simplifying assumptions in doing so. They represent emissions, chemistry, transport, and sinks of aerosols to simulate the three-dimensional distributions of particle mass and number for several aerosol species. Those distributions are then provided to the radiation scheme where they are used to correct radiative fluxes for aerosol direct effects. Cloud droplet number concentrations (CDNC) can also be computed from the aerosol distributions and used in the calculation of cloud optical properties, thus representing the first indirect effect. Representation of the second indirect effect in large-scale climate models has been attempted by parameterising precipitation formation as simple functions of the CDNC, although the value of this method is debated (Stevens and Feingold, 2009). Since second indirect effects involve adjustments of cloud distributions that are not explicitly represented in the datasets used, this study focuses on the first aerosol indirect effect only. Aerosol DRF and IRF are typically computed from two parallel model simulations, the first using present-day aerosol emissions, the second using pre-industrial aerosol emissions, and both sharing the same meteorology so that changes in radiative flux are only due to anthropogenic changes in aerosols.

From an observational point of view, the task of estimating DRF and IRF involves distributions of total aerosol and cloud retrieved from satellite instruments. Since the pre-industrial state has not been observed, the determination of the anthropogenic aerosol fraction is difficult and involves proxies for the aerosol origin, such as the size of the aerosol particles. Satellite instruments also do not offer full coverage of the Earth's aerosol distribution, as aerosol optical depths (AODs) cannot be retrieved in cloudy

ACPD
12, 20073–20111, 2012

sky and are less accurate over bright surfaces. This introduces sampling biases in the spatial and temporal statistics.

The AeroCom intercomparison project of aerosol modelling reported a DRF with respect to pre-industrial conditions, represented by the year 1750, of $-0.2 \pm 0.2\,\mathrm{Wm}^{-2}$ (Schulz et al., 2006). The latest assessment report of the Intergovernmental Panel on Climate Change (IPCC) (Forster et al., 2007) added the more uncertain impact of anthropogenic nitrate and mineral dust aerosols to reach a best estimate of the DRF of $-0.4 \pm 0.4\,\mathrm{Wm}^{-2}$. On the observational side, Kaufman et al. (2005a) estimated a DRF of $-1.4 \pm 0.4\,\mathrm{Wm}^{-2}$ over cloud-free oceans by using MODIS (Moderate Resolution Imaging Spectroradiometer) retrievals of total AOD and its fine-mode fraction (FMF), combined with DRF efficiencies. Christopher et al. (2006) provided the same estimate using a different method also limited to cloud-free oceans: they combined MODIS total AODs and CERES (Clouds and the Earth's Radiant Energy System) broadband radiative fluxes. Yu et al. (2004) and Chung et al. (2005) combined model simulations and satellite observations to estimate a DRF of -1.4 and $-1.1\,\mathrm{Wm}^{-2}$, respectively, in cloud-free conditions. Chung et al. (2005) also provided an all-sky estimate ranging from -0.6 to $-0.1\,\mathrm{Wm}^{-2}$ by using monthly distributions of satellite cloud retrievals with prescribed aerosol vertical profiles. Bellouin et al. (2005, 2008) used MODIS retrievals of total AOD combined with its FMF over oceans and model-derived anthropogenic fractions over land surfaces. Their more recent estimate of the DRF, based on MODIS collection 5 data, is $-1.3\,\mathrm{Wm}^{-2}$ globally in cloud-free conditions. Assuming no aerosol DRF in cloudy sky, they scaled the cloud-free value to obtain $-0.7\,\mathrm{Wm}^{-2}$ in all-sky conditions. In a review of measurement-based studies of the DRE, Yu et al. (2006) concludes with the top-of-atmosphere (TOA) estimates of -5.5 ± 0.2 and $-4.9 \pm 0.7\,\mathrm{Wm}^{-2}$ over cloud-free ocean and land surfaces, respectively. As noted by Forster et al. (2007), satellite-based estimates of the DRF are therefore typically stronger than those by numerical models. Bellouin et al. (2008) suggested that those differences are due to the incomplete sampling of the total aerosol distribution by satellite instruments and to differences in pre-industrial and present-day natural aerosol distributions, which are used

ACPD
12, 20073–20111, 2012

as references for the DRF in numerical models and satellite- based estimates, respectively. Myhre (2009) also attributed some of the discrepancy to changes in aerosol absorption between pre-industrial and present times, which can be accounted for in model estimates but not in satellite-derived estimates.

For the IRF, Forster et al. (2007) acknowledged that the model spread in model estimates is larger than for the DRF and give, for liquid clouds, a median estimate of $-0.7\,\mathrm{Wm}^{-2}$, with a 5–95 % confidence interval range of -0.3 to $-1.8\,\mathrm{Wm}^{-2}$. On the observational side, Quaas et al. (2008) used a combination of CERES and MODIS retrievals to estimate the IRF at only $-0.2 \pm 0.1\,\mathrm{Wm}^{-2}$. Furthermore, Quaas et al. (2009) found that constraining numerical models with satellite observations decreases the IRF estimate from models. It is debated whether the discrepancy comes from inadequate assumptions when using satellite data to estimate the IRF (Penner et al., 2011) or a genuine overestimate by climate models (Quaas et al., 2011).

Simulations by numerical aerosol models are not affected by the limited sampling of satellite retrievals. Sampling can have a large impact on DRF estimates. Bellouin et al. (2008) showed that sampling the DRF obtained from a general circulation model according to the aerosol retrieval mask of MODIS was enough to increase the globally-averaged DRF by 12 %. However, relying purely on models is a poor solution because modelling the atmospheric aerosol life cycle from emission to deposition is challenging and modelled distributions can differ markedly from observations. Assimilating satellite retrievals of aerosols into a numerical model can therefore be a useful compromise, providing full coverage while keeping a strong tie with observed aerosols. Morcrette et al. (2009) and Benedetti et al. (2009) have developed an aerosol data assimilation system within the European Centre for Medium-range Weather Forecast (ECMWF) Integrated Forecast System (IFS). Within the European Framework Programme 7 MACC (Monitoring Atmospheric Composition and Climate) and MACC-II projects, this system provides aerosol forecasts, a re-analysis which covers 2003 to 2010, and an ongoing analysis.

ACPD
12, 20073–20111, 2012

In this paper, the re-analysed aerosol distributions are used to estimate the DRF and IRF. Section 2 describes the MACC aerosol re-analysis. Section 3 then describes the process whereby total AOD is distributed among four aerosol types, including the anthropogenic fraction. Sections 4 and 5 describe how the component AODs can be used to estimate the DRE, DRF, and IRF, with results covering the re-analysed period 2003–2010. The paper concludes by discussing the strengths and weaknesses of the MACC forcing estimates, as well as listing their possible uses.

2 The MACC aerosol re-analysis

The aerosol analysis and forecast system of the ECMWF IFS consists of a forward model (Morcrette et al., 2009) and a data-assimilation module (Benedetti et al., 2009). The forward model simulates the mass of five aerosol species: mineral dust, sea-salt, sulphate, black carbon (BC), and organic matter (OM). Mineral dust and sea salt are represented by three different size classes each, and hydrophilic and hydrophobic modes of BC and OM are distinguished. This sums up to 11 model tracers. Emissions of mineral dust and sea salt depend on modelled near-surface wind speeds. For the other species, emissions are provided by inventories of sulphur dioxide and primary BC and OM. BC and OM experience ageing from hydrophobic to hydrophilic components with a time constant of 1.16 days. Sulphur dioxide oxidation into sulphate aerosol is represented by a prescribed, latitude-dependent e-folding time scale ranging from 3 days at the Equator to 8 days at the poles. Sinks include dry deposition, sedimentation, and wet scavenging by large-scale and convective precipitation. The model diagnoses total and component AODs at 17 wavelengths from 0.34 to 2.13 µm. Morcrette et al. (2009) showed that this simple model compares reasonably well with observations.

The agreement with observations improves when the aerosol data assimilation system is used, as described and validated by Benedetti et al. (2009) and Mangold et al. (2011). Data assimilation consists in the minimisation of a complicated cost-function and updates the model trajectory in order to match observations more closely. This

ACPD
12, 20073–20111, 2012

has been done by using the ECMWF four-dimensional variational assimilation method, which accounts for background and observational errors. The assimilated observation is the total AOD at 0.55 µm from MODIS, available in cloud-free conditions over dark surfaces. The model control variable, which is modified according to the outcome of the data assimilation, is the total aerosol mass-mixing ratio. It is worth noting that the assimilation modifies the modelled field not only at the point of the observation but also around it. Regions with no observations because of cloudiness or high surface reflectance will still be improved by data assimilation, but to a lesser extent than regions close to the location of assimilated data. After data assimilation, each aerosol component is corrected in proportion of its original contribution to the total aerosol mass. The modelled speciation therefore remains untouched because the assimilated total AOD can only provide a single constraint: assimilation of additional observations, such as the satellite-derived FMF, is needed to also affect the modelled speciation. Nevertheless, assimilation corrects total AOD for aerosol species that are not represented in the forward model, such as nitrate.

Data assimilation can be used to initialise a forecast when done in near-real time but an analysis can also be done in retrospect using a stable version of the model. The analysis is of interest to the estimate of aerosol forcing and is used here. The top row of Fig. 1 shows the 2003–2010 seasonal averages of total AOD at 0.55 µm as provided by the MACC re-analysis with data assimilation. Interestingly, the annual and global average AOD of 0.180 is similar to that obtained from satellite retrievals, but is larger than free-running numerical simulations, with the median total AOD in AeroCom models being 0.127 (Kinne et al., 2006).

The guiding principle of the derivation of aerosol forcing from the aerosol distributions of the MACC re-analysis is to rely first on variables that are affected by data assimilation and combine them with observational estimates of other variables, such as aerosol optical properties or cloud susceptibility to aerosol changes. Unfortunately, it is not possible to completely avoid using modelled fields that are not affected by the data

ACPD
12, 20073–20111, 2012

assimilation. For example, although the aerosol forcing estimation does not rely on aerosol speciation, it does use an associated variable, the FMF of the total AOD.

3 Identification of aerosol origin

The IFS does not provide the anthropogenic fraction of the simulated aerosols for three reasons. Firstly, the aerosol origin is not always given in emission inventories, with some sectors, such as biomass-burning activities, being the sum of both natural and anthropogenic sources. Secondly, even if emissions could be broken down by aerosol origins, the model would require double the number of tracers to keep track of that information within the simulation. That would be costly and complex when natural and anthropogenic particles interact with each other. Lastly, data assimilation is based on the total aerosol column and cannot constrain natural and anthropogenic aerosols independently.

Arguably, one could simply classify mineral dust and sea-salt as natural aerosols, and sulphate, black carbon, and organic carbon as anthropogenic aerosols. Unfortunately, this simple method gives poor results, since a significant fraction of sulphate is produced from oxidation of naturally-occurring dimethyl sulphide over the oceans, and because vegetation and other natural sources produce secondary organic aerosols over land. Instead, the aerosol origin is obtained using a modified version of the algorithm by Bellouin et al. (2008) where aerosol size is used as a proxy for aerosol origin.

The algorithm starts with the identification of the mineral dust component. The original algorithm of Bellouin et al. (2008) assumes that mineral dust aerosols are large, UV-absorbing particles with FMF smaller than 0.35 ± 0.05. Although this assumption is based on in-situ measurements of aerosol properties, it is not verified in the version of the IFS used for the MACC re-analysis. Due to assumptions made on the size of emitted mineral dust particles, a large fraction of mineral dust is located in the fine mode in the MACC aerosol reanalysis. Consequently, in this instance there is no other choice

ACPD
12, 20073–20111, 2012

than to trust the modelled speciation and use the mineral dust AOD as simulated, without further processing.

The non-dust AOD, noted τ', must now be distributed into other components. Over ocean, these components can be sea-salt and anthropogenic aerosols. The identification starts with a first guess of the sea-salt optical depth, computed from the 10 m wind speed, w, as suggested by Smirnov et al. (2003):

$$\tau_{\text{seasalt}} = 0.006w + 0.06 \text{ if } w > 5\,\text{m s}^{-1} \quad (1)$$

$$= 0 \text{ if } w < 5\,\text{m s}^{-1} \quad (2)$$

where w is taken from the IFS re-analysis. If the first guess is larger or equal to τ', then sea-salt is the only aerosol component identified in the grid-box and its AOD is τ'. Otherwise, the first guess is used to correct the non-dust FMF for the contribution of sea-salt:

$$f_{\text{corrected}} = \frac{f'\tau' - f_{\text{seasalt}}\tau_{\text{seasalt}}}{\tau' - \tau_{\text{seasalt}}} \quad (3)$$

where f' is the non-dust FMF as simulated by the IFS and f_{seasalt} is the FMF of sea-salt, assumed to be 0.3. If $f_{\text{corrected}}$ remains smaller than 0.35, the first guess for sea-salt was underestimated and sea-salt AOD is set to τ'. If however $f_{\text{corrected}}$ is larger than or equal to 0.35, then the first guess for sea-salt is retained and the anthropogenic aerosol is attributed to the remaining optical depth.

Over land, two components can be identified: anthropogenic and fine-mode natural aerosols. The identification is simply done by using regional anthropogenic fractions, denoted f_{anth} and defined as the fraction of the total aerosol optical depth due to anthropogenic aerosols. Anthropogenic fractions were obtained from Hadley Centre climate model simulations first using emissions of natural aerosols only, then both natural and anthropogenic aerosols under present-day conditions. Mineral dust is excluded from those simulations in order to obtain the anthropogenic fraction of τ', as required at this

ACPD
12, 20073–20111, 2012

stage. Regional values of the anthropogenic fraction are given in Table 1. The anthropogenic fraction is not constrained by observations but is needed as it is known that some of the fine-mode aerosols over land are of natural origin, albeit difficult to discriminate from anthropogenic fine-mode aerosols. Over land, the identification is therefore

$$\tau_{\text{anth}} = f_{\text{anth}}\ \tau' \quad (4)$$

$$\tau_{\text{fine-mode natural}} = (1 - f_{\text{anth}})\ \tau' \quad (5)$$

Note that the algorithm described above conserves the AOD, and the sum of the four component AODs remains equal to the total AOD in all gridboxes.

Resulting component AODs, averaged over the MACC re-analysis period 2003–2010, are shown in Fig. 1. Distributions show the expected patterns for each aerosol component. Anthropogenic industrial aerosols dominate in North America, Europe, and Asia. Anthropogenic biomass-burning aerosols produce the large AODs seen over Central Africa and South America. Sea-salt AOD is maximum over mid-latitude oceans where near-surface wind speeds are large. Obtaining reasonable patterns gives confidence in the algorithm but is not a validation. Unfortunately, there is no purely observational dataset currently available for validating component aerosol distributions.

Uncertainties on the component AODs first arise from uncertainties in the retrievals of total AOD that is assimilated into the model and errors in the forward modelling of total AOD. Benedetti et al. (2009) evaluates the root-mean square errors of the analysis against AERONET measurements at 41 sites for May 2003 at 0.117, but it is difficult to extend this to a global uncertainty in the MACC total AOD. Instead, the relative uncertainty of 22 % for total AODs (21 % over ocean, 23 % over land) given by Yu et al. (2006) for satellite retrievals compared to AERONET is adopted here. In addition, there are uncertainties in the parameters used in the aerosol identification algorithm, namely the constants involved in computing the first guess sea-salt AOD, the threshold on the FMF, and the regional anthropogenic fractions over land. These translate into an additional uncertainty of 15 % on the anthropogenic AOD (10 % over ocean, 17 % over land) according to the Monte-Carlo approach used by Bellouin et al. (2005). The overall

ACPD
12, 20073–20111, 2012

relative uncertainty in anthropogenic AOD is therefore 37 % (31 % over ocean, 40 % over land) and those percentages are used for all component AODs. Those values are smaller than the estimated 60 % on the anthropogenic AOD in Yu et al. (2006), which relies on an identification method where the FMF is used directly in a formula giving the anthropogenic AOD. The method used in this study only compares the FMF to a threshold and the impact of the FMF uncertainty is reduced.

Table 2 gives total and component AODs and their uncertainties for the MACC estimates. The globally and annually-averaged total and anthropogenic AODs at 0.55 µm are 0.180 ± 0.040 and 0.048 ± 0.018, respectively. On a global average, sea-salt contributes most (44 %) to the total AOD, with an annual average of 0.080 ± 0.030. Anthropogenic aerosols represent 27 % of the total AOD. Bellouin et al. (2008) obtained a similar anthropogenic AOD of 0.043 for the year 2002 using MODIS collection 5 aerosol retrievals, 23 % of their total AOD. On the modelling side, AeroCom models simulate an anthropogenic AOD of 0.036 (Schulz et al., 2006), or 31 % of their present-day total AOD. Here, the AeroCom anthropogenic AOD of 0.029, defined with respect to pre-industrial conditions, has been multiplied by 1.25 to correct for the pre-industrial aerosol distribution, following Bellouin et al. (2008) where aerosol and precursor emissions for the year 1860 were used to represent pre-industrial aerosols. There is therefore some agreement in the fraction of present-day total AOD that is anthropogenic between satellite-based, assimilation-based, and modelling-based estimates. However, free-running global aerosol models have lower total and anthropogenic AODs.

4 Aerosol direct effect and forcing

4.1 Aerosol direct effect

Now that component AODs are known, radiative transfer calculations are needed to obtain direct effects. DREs are computed for all four aerosol components identified by the algorithm with respect to an atmosphere containing no aerosols. Radiative transfer

ACPD
12, 20073–20111, 2012

calculations require the knowledge of the aerosol optical properties, the surface albedo, and the cloud and aerosol vertical profile. Aerosol radiative effects and forcing are only estimated in the shortwave spectrum. The aerosol vertical profile is a key parameter in the longwave spectrum. The modelled profile cannot be relied upon, however, since it is unaffected by data assimilation.

Aerosol optical properties are derived from size distributions and single-scattering albedos retrieved from ground-based sun-photometer measurements at specific sites worldwide (Dubovik et al., 2002); such sites are assumed to be representative either of a given aerosol type (mineral dust, sea-salt, and fine-mode natural aerosols) or of a regional anthropogenic aerosol. Representative sites and single-scattering albedo values are given in Table 1. The regions are the same as used for prescribing the anthropogenic fraction in the previous section. The fine-mode natural aerosol is assumed to have a single-scattering albedo of 0.98 at 0.55 µm and the same size distribution as the North American aerosol. Prescribed aerosol absorption properties yield the seasonal distributions of absorption AOD shown in Fig. 2. Anthropogenic aerosols contribute most to the absorption, which is located predominantly in the Southern Hemisphere and Asia. On a global average, the single-scattering albedo is 0.97.

Surface albedo is computed over ocean as a function of solar zenith angle and 10 m wind speed (Cox and Munk, 1954) and taken from the IFS over land in the visible and near-infrared spectra.

The aerosol vertical profile is not taken from the IFS since that aspect of the model is unaffected by data assimilation. Rather, it is assumed that natural aerosols are located in the first kilometre of the atmosphere, below a layer of anthropogenic aerosols. For the cloud-free DRE, the impact of this assumed vertical profile on shortwave radiative fluxes is small: the change in molecular scattering above the aerosol layer is a second-order effect.

Radiative transfer calculations are performed using a discrete-ordinate solver (Key and Schweiger, 1998), with 24 shortwave wavebands and 24 streams. The 24 h averaged DRE is computed by integrating the instantaneous radiative effects over the

ACPD
12, 20073–20111, 2012

solar zenith angles as a function of latitude and day of the year, with 10 timesteps per day.

Total and component DREs in the shortwave spectrum in cloud-free sky at the TOA, averaged over the MACC re-analysis period, are shown in Fig. 3. Component DREs follow the distribution of the corresponding component AOD but with strengths modulated by aerosol absorption properties and surface albedo. In both hemispheres, total DRE is stronger during the summer when incoming solar radiation is larger. Consequently, the globally-averaged total DRE is stronger during the Northern Hemisphere summer, as more aerosols are located in the Northern Hemisphere. DREs and direct radiative effect efficiencies (DREEs) are given in Table 2 for TOA and surface, averaged over the MACC re-analysis period. Efficiencies are within previously-published ranges (Anderson et al., 2005; Yu et al., 2006). Varying efficiencies reflect the different absorbing properties of the different species. At the TOA, DREE decreases with increasing aerosol absorption, since absorption does not reflect radiation back to space. In constrast, at the surface, DREE increases with increasing aerosol absorption, since none of the absorbed radiation reaches the surface, unlike scattered radiation that may still do so from another direction. Differences in surface albedo where some species are preferentially located also matter. Anthropogenic aerosols are less efficient than sea-salt at exerting a direct effect at the TOA, and their contribution of 24 % to the total direct effect is therefore less than their contribution of 28 % to the total AOD. At the surface, both anthropogenic and sea-salt aerosols contribute almost equally to the total direct effect, at 40 % each.

The difference between TOA and surface forcing gives the amount of energy absorbed in the atmosphere because of the aerosols, sometimes termed atmospheric forcing. On an annual basis, this is estimated here at $+2.6\,\mathrm{Wm}^{-2}$. Anthropogenic aerosols absorption represents $+2.1\,\mathrm{Wm}^{-2}$ (81 %) of the total, with the remainder being associated to mineral dust and fine-mode natural aerosols. As expected from the distribution of anthropogenic aerosols, most of aerosol absorption is located over land.

ACPD
12, 20073–20111, 2012

Uncertainties in the DRE arise from uncertainties in component optical depths and uncertainties in the prescribed regional optical properties, especially absorption. Uncertainties in component AOD, computed above, are translated to uncertainties in component DRE by multiplying by the component DREE. In addition, the uncertainty on the DREE due to uncertain prescribed optical properties has been quantified for the anthropogenic component by the Monte-Carlo approach of Bellouin et al. (2005), who obtained absolute uncertainties of 0.3 (0.1 over ocean, 0.9 over land) Wm^{-2} at the TOA and 0.6 (0.4 over ocean, 1.2 over land) Wm^{-2} at the surface. Taking the overall uncertainty in anthropogenic DRE as the sum of the uncertainty due to uncertain component AODs and to uncertain optical properties, the relative uncertainty becomes 55 % (38 % over ocean, 68 % over land) at the TOA.

In Yu et al. (2006), the cloud-free DRE is estimated over oceans at $-5.5 \pm 0.2\,Wm^{-2}$ at the TOA and $-8.8 \pm 0.7\,Wm^{-2}$ at the surface, where uncertainties are a measure of diversity among different satellite-based methods rather than an actual measure of the overall uncertainty as attempted in this study. The corresponding MACC estimates, listed in Table 2, are stronger at -8.0 ± 3.1 and $-9.6 \pm 4.4\,Wm^{-2}$, respectively. In addition to the problem of incomplete sampling of aerosol distributions by satellite products, stronger values can be explained by three different factors. Firstly, the total AOD over ocean is larger in MACC, at 0.17, than in Yu et al. (2006), at 0.14: in the same environmental conditions, larger AODs exert stronger DREs. Secondly, more of the total AOD is identified as sea-salt in MACC, where the cloud-free anthropogenic fraction of the total AOD is 16 %, compared to 21 % in Yu et al. (2006): scattering sea-salt aerosols are more efficient at exerting a forcing at the TOA than more absorbing species. Thirdly, the MACC total DRE is computed as the sum of the component DREs: this method neglects the coupling between the DRE of different species and overestimates the DRE by a few tenths of Wm^{-2}, the exact value depending on the relative vertical profiles of the different aerosol species. Over cloud-free land, Yu et al. (2006) gives $-4.9 \pm 0.7\,Wm^{-2}$ at the TOA and $-11.8 \pm 1.9\,Wm^{-2}$ at the surface, for a total

ACPD
12, 20073–20111, 2012

AOD of 0.220. Corresponding MACC values are -6.4 ± 4.3 and $-11.5 \pm 6.6\,\mathrm{Wm}^{-2}$, for a total AOD of 0.203.

4.2 Aerosol direct forcing

The direct forcing is computed for anthropogenic aerosols as the difference between an atmosphere containing all aerosols and an atmosphere containing natural aerosols only. In effect, natural aerosols therefore act as a proxy for pre-industrial aerosols. Calculations are similar to that for the direct effect, as described in the previous section. One difference worth noting is the impact of the prescribed vertical profile. For the direct forcing, the direct effect of natural aerosols modifies the radiative fluxes experienced by anthropogenic aerosols, and therefore their forcing. The assumption that natural aerosols are located below the anthropogenic layer effectively increases the reflectance of the underlying atmosphere, and makes the DRF less negative than when other vertical profiles are used.

The top row of Fig. 4 shows the cloud-free estimates of DRF, seasonally over the period 2003–2010. The global, multi-annual average is $-1.6\,\mathrm{Wm}^{-2}$ at the TOA, and $-3.6\,\mathrm{Wm}^{-2}$ at the surface. Relative uncertainties in the DRF are assumed to be the same as for the DRE (55 %) and are used to compute absolute uncertainties listed in Table 4 with ocean and land averages. Direct forcing is typically stronger over continents and in the Northern Hemisphere, where most anthropogenic sources are located, and in Northern Hemisphere summer, when both anthropogenic AOD and incoming solar radiation are largest.

The aerosol DRF is scaled from cloud-free to all-sky conditions by multiplying, in each gridbox, the cloud-free DRF by the cloud-free fraction simulated by the IFS. Doing so yields an all-sky DRF of $-0.5\,\mathrm{Wm}^{-2}$ (see Table 4) and is equivalent to assuming a DRF of zero in cloudy sky. This assumption is known to be wrong, however, as aerosols overlying clouds may exert a sizeable DRF, which is positive for absorbing aerosols, as recently estimated from remote sensing off the Western African coast (de

ACPD
12, 20073–20111, 2012

Graaf et al., 2012). AeroCom models simulate a globally-averaged cloudy-sky DRF of −0.2 to +0.3 Wm^{-2} (Schulz et al., 2006). Bellouin et al. (2008) showed that in the Hadley Centre climate model, the all-sky DRF is −0.5 Wm^{-2} if cloudy-sky DRF is taken to be zero, 1.7 times stronger than the actual all-sky DRF of −0.3 Wm^{-2}. Based on that model, we apply a correction term of $+0.1 \pm 0.1\,Wm^{-2}$ for aerosol absorption in cloudy sky. Accounting for both the 55 % ($\pm 0.3\,Wm^{-2}$) uncertainty on the all-sky DRF coming directly from the cloud-free estimate and the correction for cloudy-sky forcing, all-sky DRF is $-0.4 \pm 0.4\,Wm^{-2}$ or, expressed in terms of lower and upper bounds, −0.8 to 0 Wm^{-2}. The DRF uncertainty analysis is summarised in Table 3.

The MACC estimate of all-sky DRF has to be corrected further before comparing against model and IPCC estimates. This correction addresses the difference between present-day natural aerosols and pre-industrial aerosols when acting as the reference state for the forcing. Bellouin et al. (2008) applied both reference states in the Hadley Centre climate model and found that, for the same present-day anthropogenic aerosol distribution, the all-sky DRF is 1.6 times weaker when pre-industrial aerosols, represented by the year 1860, are used as a reference. Using that factor, the MACC estimate of all-sky DRF with respect to pre-industrial becomes −0.3 Wm^{-2}, bounded by −0.5 and 0 Wm^{-2}. The best estimate is within the AeroCom (Schulz et al., 2006) and IPCC (Forster et al., 2007) estimates of -0.2 ± 0.2 and $-0.4 \pm 0.4\,Wm^{-2}$, respectively.

5 Aerosol indirect forcing

The IRF is the change in cloud albedo exerted by a change in cloud droplet number concentration due to anthropogenic aerosols. The MACC estimate follows the method of Quaas et al. (2008) where IRF is computed as:

$$\mathrm{IRF} = f_{\mathrm{cld,liq}} \overline{F}_{\downarrow} \frac{\partial \alpha}{\partial \ln N_d} \frac{\partial \ln N_d}{\partial \ln \tau} (\ln \tau - \ln \tau_{\mathrm{nat}}) \quad (6)$$

where:

ACPD
12, 20073–20111, 2012

- $f_{\mathrm{cld,liq}}$ is the projected fractional cover of liquid clouds, that is clouds that have liquid water rather than ice at their tops and are not obscured by overlying ice clouds. In this study, cloud cover is the low-level cloud cover, for clouds whose top pressures are above 680 hPa, as diagnosed by the IFS. No attempts are made to estimate the IRF of ice clouds. In order to avoid having ice clouds among the low-level clouds, indirect forcing is not calculated for regions poleward of 60°.

- $\overline{F}_{\downarrow}$ is the daily-mean incoming solar radiative flux, in Wm^{-2}, at the top of the atmosphere, computed from the declination angle and Earth–Sun distance corresponding to the Julian day of the year and from the length of day corresponding to the latitude and day of the year;

- α is the broadband shortwave planetary albedo;

- N_d is the liquid CDNC;

- τ is the AOD;

- τ_{nat} is the natural AOD, derived from the anthropogenic AOD as estimated above.

The two partial derivatives are the key terms in the estimate of IRF and are taken from the statistical analysis of satellite retrievals performed by Quaas et al. (2008).

The first derivative, $\partial\alpha/\partial \ln N_d$, is the sensitivity of liquid cloud albedo to a relative change in CDNC. This sensitivity depends on cloud fraction and cloud optical depth and is computed using the statistical method of Quaas et al. (2008), except that the cloud cover used here is simulated by the IFS. IFS does not diagnose cloud optical depth, however, and it is instead computed from the diagnosed cloud liquid water path assuming vertically homogeneous clouds with an effective droplet radius of 10 µm.

The second derivative is the sensitivity of CDNC to a relative change in AOD. In principle, CDNC is a function of cloud condensation nuclei (CCN) number concentrations and cloud-scale updraft velocity as described by Köhler theory. At the large scale however, a parameterisation needs to reflect the bulk effect of aerosol concentrations on

ACPD
12, 20073–20111, 2012

cloud droplet number concentrations (e.g. Lohmann et al., 2007). Here we choose to use AOD as a proxy for CCN number concentrations (Andreae, 2009). Since relative changes are considered, it is sufficient if CCN scale with AOD.

There has recently been a debate in the literature on the validity of the statistical approach used to estimate the IRF (Penner et al., 2011; Quaas et al., 2011). Specifically, it was questioned whether the sensitivity of CDNC for a perturbation of AOD is a metric able to capture the real change in CDNC from pre-industrial to present-day times (McComiskey et al., 2009). There are suggestions that the choice of AOD as a proxy for CCN number concentrations (Andreae, 2009) leads to an underestimation of aerosol indirect radiative forcing (Penner et al., 2011). Inversely, Grandey and Stier (2010) suggest that the statistical method by Quaas et al. (2008), also used here, leads to an overestimation. Given the available data, the method is considered valid for this work, but an uncertainty assessment is important.

In the evaluation of Eq. (6), the sensitivity of cloud albedo to CDNC changes and the sensitivity of CDNC to AOD changes are taken from an analysis of satellite observations, where solar broadband albedo is taken from CERES (Wielicki et al., 1996; Loeb et al., 2002) retrievals, and AOD and cloud properties are retrieved by MODIS (Remer et al., 2005; Minnis et al., 2003). CDNC is estimated from cloud optical depth and cloud effective radius assuming adiabatic clouds, following Quaas et al. (2006). The partial derivatives are evaluated as in Quaas et al. (2008) for fourteen different oceanic and continental regions, and the four seasons of the year.

Seasonal distributions of all-sky IRF at TOA are shown in the third row of Fig. 4. IRF is stronger where aerosols interact with low, maritime clouds. This includes the stratocumulus decks off the coasts of Namibia, California, and Peru. Over land, IRF is weak. On a multi-annual, global average, the best estimate of IRF is $-0.4\,\mathrm{Wm}^{-2}$.

As done for the DRF, the IRF uncertainty assessment aims at producing the full uncertainty range. For the individual factors in Eq. (6), errors in the simulated fractional cover by liquid clouds and in daily-mean incoming solar radiation are considered negligible compared to errors in the three remaining factors. For the sensitivity of cloud

ACPD
12, 20073–20111, 2012

albedo to a change in CDNC, the seasons with the largest and smallest sensitivity are selected as boundaries in each region. The uncertainty assessment further includes errors due to the assumption of constant effective radius in the computation of the cloud optical thickness, varying the assumed effective radius in the IFS between 5 and 20 µm. The most uncertain factor in the equation is likely to be the sensitivity of CDNC to changes in AOD. This term has been investigated from satellite- and ground-based remote sensing in several studies. Two recent review studies report the range of values found by different investigators (Nakajima and Schulz, 2009; McComiskey and Feingold, 2012). To explore the uncertainty range in each region, the smallest and largest sensitivities in the range of physically plausible (i.e. positive) values are taken from those compilations. Over ocean, maximum sensitivities are 0.927 in the 20–30° S belt (Kaufman et al., 2005b) and 0.771 elsewhere (Nakajima et al., 2001). Over land, maximum sensitivity is 0.471 (Myhre et al., 2007). Minimum sensitivities are 0.120 over ocean and 0.036 over land (Quaas et al., 2004). Finally, the relative change in aerosol optical depth due to anthropogenic emissions has the relative error of 37 % considered above for the DRF. It is worth noting that this error is bounded by zero and the total AOD, since anthropogenic AOD cannot be negative or exceed total AOD. Table 5 summarises the uncertainty analysis for the first indirect forcing. As expected, CDNC sensitivity brings the largest uncertainties. The overall range of IRF estimates is −2.1 to $-0.1\,\mathrm{Wm}^{-2}$ (Table 4), encompassing both stronger and weaker values than the 5–95 % confidence range of −1.8 to $-0.3\,\mathrm{Wm}^{-2}$ assessed by the IPCC (Forster et al., 2007). Figure 5 shows distributions of the strongest, best, and weakest estimates of multi-annual averaged IRF.

6 Total aerosol forcing

Total aerosol forcing is defined as the sum of DRF and IRF. Seasonal distributions of all-sky total forcing at the TOA over the period 2003–2010 are shown in the bottom row of Fig. 4. Total forcing is dominated by DRF and is therefore predominantly located over

ACPD
12, 20073–20111, 2012

land. IRF dominates over oceanic stratocumulus deck regions. Table 4 gives the best estimate of globally-averaged total forcing at $-0.9\,\mathrm{Wm}^{-2}$. This value is uncorrected for differences between present-day natural and pre-industrial aerosol distributions because such a correction has only been applied to the DRF.

The large uncertainties in DRF and IRF estimates translate, if combined linearly and assumed independent, to an uncertainty range of -2.9 to $-0.1\,\mathrm{Wm}^{-2}$ for the total forcing. This range is very similar to the distribution function obtained by the fourth IPCC assessment report, where probability peaks at $-1\,\mathrm{Wm}^{-2}$ but is non-zero over the range -3.0 to $0\,\mathrm{Wm}^{-2}$ (see Fig. 2.20 of Forster et al., 2007). The MACC estimates can therefore be interpreted as an independently-derived confirmation of the IPCC range, although the uncertainty range has not been reduced.

7 Conclusions

Estimation of aerosol forcing from the MACC aerosol re-analysis uses data-assimilated aerosol products from ECMWF in order to combine the strengths of satellite-based estimates, which are tied to actual aerosol distributions, with free-running model estimates, which do not include data gaps and may provide additional information. The globally-averaged anthropogenic AOD over the period 2003–2010 is 0.048 ± 0.018. Its uncertainty is dominated by that on the satellite retrieval of total AOD. Clear-sky anthropogenic DRE is $-1.8 \pm 1.0\,\mathrm{Wm}^{-2}$ at the TOA. Uncertainty on the anthropogenic AOD dominates the overall uncertainty, with $\pm 0.7\,\mathrm{Wm}^{-2}$. Clear-sky anthropogenic DRF is $-1.6 \pm 0.9\,\mathrm{Wm}^{-2}$ at the TOA and shares the same relative uncertainty as the clear-sky anthropogenic DRE. The best estimate of all-sky anthropogenic DRF is $-0.5\,\mathrm{Wm}^{-2}$, or $-0.3\,\mathrm{Wm}^{-2}$ if differences between present-day natural and pre-industrial aerosols are taken into account. The uncertainty range is -0.8 to $0\,\mathrm{Wm}^{-2}$, with most of the uncertainty coming from the clear-sky estimate. Best estimate of all-sky IRF is $-0.4\,\mathrm{Wm}^{-2}$. The uncertainty range is -2.1 to $-0.1\,\mathrm{Wm}^{-2}$ and is dominated by the uncertainty in the CDNC susceptibility to anthropogenic changes in AOD. Although uncertainty ranges

ACPD
12, 20073–20111, 2012

derived in this study are similar to those obtained by the fourth IPCC assessment report (Forster et al., 2007), the best estimate of IRF is much weaker.

The MACC aerosol products are not observations of aerosol radiative effects and forcings. The estimates are obtained by radiative transfer modelling and based on a number of simplifying assumptions. The anthropogenic AOD, for example, is in fact a size-based proxy for the actual anthropogenic AOD, which may never be derived from observations. However, the aerosol forcing products created as part of the MACC project represent a beneficial combination of the strengths of observationally-based and modelled-based estimates. Satellite estimates have the advantage of relying on observations, but for various reasons cannot offer a complete temporal and spatial coverage of the Earth's surface, thus introducing sampling biases in their statistics. Modelled estimates offer such a complete coverage, but can fail in simulating the complexity of real aerosol distributions. MACC aerosol forcing products are observationally-based within a model framework. The MACC aerosol reanalysis assimilates satellite aerosol retrievals to correct for model errors in simulating the total and fine-mode aerosol optical depths. The aerosol forcings are derived from those AODs and therefore benefit from the assimilation directly. Most other aerosol properties needed in the forcing estimates are also based on observations. For the direct forcing, size distributions and scattering and absorbing properties are taken from ground-based sun-photometer measurements. For the first indirect forcing, cloud susceptibilities to changes in aerosols are derived from satellite measurements.

In addition to providing another estimate of aerosol radiative effects and forcings, the MACC aerosol products have a variety of possible uses. First, they can provide corrections of surface fluxes for the radiative effects of natural and anthropogenic aerosols that typically decrease the downward shortwave flux reaching the surface. Scientists or engineers interested in the surface energy budget (e.g. hydrological cycle), vegetation and ecosystem services (e.g. carbon cycle) or solar energy can use the products to correct for changes in surface radiative fluxes due to the effect of aerosols. Second, MACC products can provide patterns of aerosol radiative forcing for detection and

ACPD
12, 20073–20111, 2012

attribution studies using optimal finger printing techniques. Although those techniques can correct for errors in the magnitude of anthropogenic and natural forcings, they require the knowledge of spatial and temporal patterns of specific forcing agents. Third, MACC products can provide initial conditions for seasonal and decadal forecasts, which require a good knowledge of the boundary conditions of the climate system. These include regional forcings due to short-lived species which can evolve during the forecast period. The MACC forcing products provide the aerosol contribution to such a forcing, and how that contribution has changed in the recent past, which is useful for hindcast simulations, and by extrapolation how it is likely to evolve in the near future. Fourth, MACC products can deliver trends in aerosol forcing. On a global scale, aerosol climate forcing is negative and offsets part of the positive forcing by greenhouse gases. A weaker aerosol forcing in the future would leave an increasing fraction of greenhouse gas forcing unopposed, exacerbating global warming (Andreae et al., 2000). Trends in aerosol radiative forcing for 2003–2010 are shown in Fig. 6. Weaker aerosol forcing over North America, Europe, and Central Africa is due to anthropogenic AOD getting smaller over those regions. In contrast, DRF from increasing anthropogenic AOD is getting stronger over Western Russia, Central China, and Central Pacific Ocean. Trends over the Southern Atlantic and Indian oceans come from stronger DRF from transported biomass-burning activities in South America and Africa, respectively. Negative trends over the Southern Pacific Ocean are not associated with large changes in anthropogenic AOD. Instead, they arise from the IRF, and may be linked to changes in low cloud cover. As the MACC analysis extends into the future, the MACC forcing products will provide increasingly robust trends in anthropogenic aerosol amounts and forcing, which will help to understand warming trends. However, care should be exercised when looking at trends in the current MACC products, especially at the global scale, because the satellite data which are assimilated in the aerosol monitoring system are known to have spurious trends due to calibration issues. Finally, the MACC aerosol products can help in measuring the climate impacts of air quality policies. Air quality regulations aimed at improving human health have led to a strong decrease in anthropogenic

ACPD
12, 20073–20111, 2012

emissions of aerosols and their precursors in Europe and North America, followed by a decrease in particulate matter and an improvement in air quality. Emerging countries are likely to enact similar regulations in the future. A decrease in the concentration of most aerosol types translates into the removal of a cooling influence on climate, which can be assessed using MACC aerosol products.

Two planned improvements to the MACC aerosol data assimilation system are expected to bring important benefits to the estimation of aerosol forcing. First, the assimilation of MODIS aerosol fine-mode fractions will increase confidence in the anthropogenic AOD. Second, the assimilation of aerosol vertical profiles from the Cloud-Aerosol Lidar with Orthogonal Polarisation (CALIOP) satellite instrument will allow the estimation of aerosol direct effects in cloudy sky. In addition, land-based anthropogenic fractions, and regional datasets of single-scattering albedo of anthropogenic aerosols are currently prescribed over large regions (Table 1). Those will be replaced by gridded datasets derived from an extended analysis of sun-photometer measurements and AeroCom model simulations.

Daily distributions and monthly browses of aerosol radiative effects and forcing are freely available at www.gmes-atmosphere.eu/d/services/gac/reanalysis/forcing. Products are currently available for the period 2003–2010, in netCDF format, and the database will be extended regularly as the MACC aerosol analysis progresses.

Acknowledgements. This work is funded by the Monitoring Atmospheric Composition and Climate (MACC) II project of the European Commission under the European Union Seventh Framework Programme, grant agreement number 283576, and supported by the Joint DECC/Defra Met Office Hadley Centre Climate Programme (GA01101).

References

Anderson, T. L., Charlson, R. J., Bellouin, N., Boucher, O., Chin, M., Christopher, S. A., Haywood, J., Kaufman, Y. J., Kinne, S., Ogren, J. A., Remer, L. A., Takemura, T., Tanre, D., Torres, O., Trepte, C. R., Wielicki, B. A., Winker, D. A., and Yu, H.: An "A-Train" strategy

ACPD
12, 20073–20111, 2012

for quantifying direct climate forcing by anthropogenic aerosols, B. Am. Meteorol. Soc., 12, 1795–1809, 2005. 20085

Andreae, M. O.: Correlation between cloud condensation nuclei concentration and aerosol optical thickness in remote and polluted regions, Atmos. Chem. Phys., 9, 543–556, doi:10.5194/acp-9-543-2009, 2009. 20090

Andreae, M. O., Jones, C. D., and Cox, P. M.: Strong present-day aerosol cooling implies a hot future, Nature, 435, 1187–1190, 2005. 20094

Bellouin, N., Boucher, O., Haywood, J., and Reddy, M. S.: Global estimate of aerosol direct radiative forcing from satellite measurements, Nature, 438, 1138–1141, 2005. 20076, 20082, 20086, 20103

Bellouin, N., Jones, A., Haywood, J., and Christopher, S. A.: Updated estimate of aerosol direct radiative forcing from satellite observations and comparison against the Hadley Centre climate model, J. Geophys. Res., 113, D10205, doi:10.1029/2007JD009385, 2008. 20076, 20077, 20080, 20083, 20088, 20103

Benedetti, A., Morcrette, J.-J., Boucher, O., Dethof, A., Engelen, R.J., Fisher, M., Flentje, H., Huneeus, N., Jones, L., Kaiser, J. W., Kinne, S., Mangold, A., Razinger, M., Simmons, A. J., and Suttie, M.: Aerosol analysis and forecast in the ECMWF integrated forecast system: 2. Data assimilation, J. Geophys. Res., 114, D13205, doi:10.1029/2008JD011115, 2009. 20077, 20078, 20082

Christopher, S. A., Zhang, J., Kaufman, Y. J., and Remer, L. A.: Satellite-based assessment of top of atmosphere anthropogenic aerosol radiative forcing over cloud-free oceans, Geophys. Res. Lett., 33, L15816, doi:10.1029/2005GL025535, 2006. 20076

Chung, C. E., Ramanathan, V., Kim, D., and Podgorny, I. A.: Global anthropogenic aerosol direct forcing derived from satellite and ground-based observations, J. Geophys. Res., 110, D24207, doi:10.1029/2005JD006356, 2005. 20076

Cox, C. and Munk, W.: Statistics of the sea surface derived from sun glitter. J. Mar. Res., 13, 198–227, 1954. 20084

de Graaf, M., Tilstra, L. G., Wang, P., and Stammes, P.: Retrieval of the aerosol direct radiative effect over clouds from spaceborne spectrometry, J. Geophys. Res., 117, D07207, doi:10.1029/2011JD017160, 2012. 20087

Dubovik, O., Holben, B., Eck, T. F., Smirnov, A., Kaufman, Y. J., King, M. D., Tanre, D., and Slutsker, I.: Variability of absorption and optical properties of key aerosol types observed in worldwide locations, J. Atmos. Sci., 59, 590–608, 2002. 20084, 20101

ACPD

12, 20073–20111, 2012

Forster, P., Ramaswamy, V., Artaxo, P., Berntsen, T., Betts, R., Fahey, D. W., Haywood, J., Lean, J., Lowe, D. C., Myhre, G., Nganga, J., Prinn, R., Raga, G., Schulz, M., and Van Dorland, R.: Changes in atmospheric constituents and in radiative forcing, in: Climate Change 2007: The Physical Science Basis, Contribution of Working Group I to the Fourth Assessment Report of the Intergovernmental Panel on Climate Change, edited by: Solomon, S., Qin, D., Manning, M., Chen, Z., Marquis, M., Averyt, K. B., Tignor, M., and Miller, H. L., Cambridge Univ. Press, New York, 2007. 20075, 20076, 20077, 20088, 20091, 20092, 20093

Grandey, B. S. and Stier, P.: A critical look at spatial scale choices in satellite-based aerosol indirect effect studies, Atmos. Chem. Phys., 10, 11459–11470, doi:10.5194/acp-10-11459-2010, 2010. 20090

Kaufman, Y. J., Boucher, O., Tanre, D., Chin, M., Remer, L. A., and Takemura, T.: Aerosol anthropogenic component estimated from satellite data, Geophys. Res. Lett., 32, L17804, doi:10.1029/2005GL023125, 2005a. 20076

Kaufman, Y. J., Koren, I., Remer, L. A., Rosenfeld, D., and Rudich, Y.: The effect of smoke, dust, and pollution aerosol on shallow cloud development over the Atlantic Ocean, P. Natl. Acad. Sci. USA, 102, 11207–11212, 2005b. 20091

Key, J. R. and Schweiger, A. J.: Tools for atmospheric radiative transfer: STREAMER and FLUXNET, Comput. Geosci., 24, 443–451, 1998. 20084

Kinne, S., Schulz, M., Textor, C., Guibert, S., Balkanski, Y., Bauer, S. E., Berntsen, T., Berglen, T. F., Boucher, O., Chin, M., Collins, W., Dentener, F., Diehl, T., Easter, R., Feichter, J., Fillmore, D., Ghan, S., Ginoux, P., Gong, S., Grini, A., Hendricks, J., Herzog, M., Horowitz, L., Isaksen, I., Iversen, T., Kirkevåg, A., Kloster, S., Koch, D., Kristjansson, J. E., Krol, M., Lauer, A., Lamarque, J. F., Lesins, G., Liu, X., Lohmann, U., Montanaro, V., Myhre, G., Penner, J., Pitari, G., Reddy, S., Seland, O., Stier, P., Takemura, T., and Tie, X.: An AeroCom initial assessment – optical properties in aerosol component modules of global models, Atmos. Chem. Phys., 6, 1815–1834, doi:10.5194/acp-6-1815-2006, 2006. 20079

Loeb, N. G., Kato, S., and Wielicki, B. A.: Defining top-of-the-atmosphere flux reference level for Earth radiation budget experiments, J. Climate, 15, 3302–3309, 2002. 20090

Lohmann, U., Quaas, J., Kinne, S., and Feichter, J.: Different approaches for constraining global climate models of the anthropogenic indirect aerosol effect, B. Am. Meteorol. Soc., 88, 243–249, 2007. 20090

Mangold, A., De Backer, H., De paepe, B., Ceburnis, D., Chiapello, I., Derimian, Y., Flentje, H., Huneeus, N., Kinne, S., Morcrette, J.-J., Benedetti, A., and Boucher, O.: Aerosol analysis

ACPD
12, 20073–20111, 2012

and forecast in the ECMWF Integrated Forecast System, Part III: Evaluation by means of case studies, J. Geophys. Res., 116, D03302, doi:10.1029/2010JD014864, 2011. 20078

McComiskey, A. and Feingold, G.: The scale problem in quantifying aerosol indirect effects, Atmos. Chem. Phys., 12, 1031–1049, doi:10.5194/acp-12-1031-2012, 2012. 20091

McComiskey, A., Feingold, G., Frisch, A. S., Turner, D., Miller, M., Chiu, J., Min, Q., and Ogren, J.: An assessment of aerosol-cloud interactions in marine stratus clouds based on surface remote sensing, J. Geophys. Res., 114, D09203, doi:10.1029/2008JD011006, 2009. 20090

Minnis, P., Young, D. F., Sun-Mack, S., Heck, P. W., Doelling, D. R., and Trepte, Q. Z.: CERES cloud property retrievals from imagers on TRMM, Terra, and Aqua, in: Proc. SPIE 10th International Symposium on Remote Sensing: Conference on Remote Sensing of Clouds and the Atmosphere VII, vol. 5235, Barcelona, Spain, 37–48, 2003. 20090

Morcrette, J.-J., Boucher, O., Jones, L., Salmond, D., Bechtold, P., Beljaars, A., Benedetti, A., Bonet, A., Kaiser, J. W., Razinger, M., Schulz, M., Serrar, S., Simmons, A. J., Sofiev, M., Suttie, M., Tompkins, A. M., and Untch, A.: Aerosol analysis and forecast in the ECMWF integrated forecast system: forward modeling, J. Geophys. Res., 114, D06206, doi:10.1029/2008JD011235, 2009. 20077, 20078

Myhre, G.: Consistency between satellite-derived and modeled estimates of the direct aerosol effect, Science, 325, 187–190, 2009. 20077

Myhre, G., Stordal, F., Johnsrud, M., Kaufman, Y. J., Rosenfeld, D., Storelvmo, T., Kristjansson, J. E., Berntsen, T. K., Myhre, A., and Isaksen, I. S. A.: Aerosol-cloud interaction inferred from MODIS satellite data and global aerosol models, Atmos. Chem. Phys., 7, 3081–3101, doi:10.5194/acp-7-3081-2007, 2007. 20091

Nakajima, T. and Schulz, M.: What do we know about large-scale changes of aerosols, clouds, and the radiation budget?, in: Clouds and the Perturbed Climate System, Ernst Strüngmann Forum, edited by: Heintzenberg, J. and Charlson, R. J., ISBN 978-0-262-01287-4, MIT Press, Cambridge, 2009. 20091

Nakajima, T., Higurashi, A., Kawamoto, K., and Penner, J. E.: A possible correlation between satellite-derived cloud and aerosol microphysical parameters, Geophys. Res. Lett., 28, 1171–1174, 2001. 20091

Penner, J. E., Xu, L., and Wang, M.: Satellite methods underestimate indirect climate forcing by aerosols, P. Natl. Acad. Sci. USA, 108, 13404–13408, doi:10.1073/pnas.1018526108, 2011. 20077, 20090

ACPD

12, 20073–20111, 2012

Quaas, J., Boucher, O., and Bréon, F.-M.: Aerosol indirect effects in POLDER satellite data and in the LMDZ GCM, J. Geophys. Res., 106, 31991–32004, 2004. 20091

Quaas, J., Boucher, O., and Lohmann, U.: Constraining the total aerosol indirect effect in the LMDZ and ECHAM4 GCMs using MODIS satellite data, Atmos. Chem. Phys., 6, 947–955, doi:10.5194/acp-6-947-2006, 2006. 20090

Quaas, J., Boucher, O., Bellouin, N., and Kinne, S.: Satellite-based estimate of the direct and indirect aerosol climate forcing, J. Geophys. Res., 113, D05204, doi:10.1029/2007JD008962, 2008. 20077, 20088, 20089, 20090

Quaas, J., Ming, Y., Menon, S., Takemura, T., Wang, M., Penner, J. E., Gettelman, A., Lohmann, U., Bellouin, N., Boucher, O., Sayer, A. M., Thomas, G. E., McComiskey, A., Feingold, G., Hoose, C., Kristjánsson, J. E., Liu, X., Balkanski, Y., Donner, L. J., Ginoux, P. A., Stier, P., Grandey, B., Feichter, J., Sednev, I., Bauer, S. E., Koch, D., Grainger, R. G., Kirkevåg, A., Iversen, T., Seland, Ø., Easter, R., Ghan, S. J., Rasch, P. J., Morrison, H., Lamarque, J.-F., Iacono, M. J., Kinne, S., and Schulz, M.: Aerosol indirect effects – general circulation model intercomparison and evaluation with satellite data, Atmos. Chem. Phys., 9, 8697–8717, doi:10.5194/acp-9-8697-2009, 2009. 20077

Quaas, J., Boucher, O., Bellouin, N., and Kinne, S.: Which of satellite- or model-based estimates is closer to reality for aerosol indirect forcing? – Reply to Penner, J. E., Xu, L., and Wang, M., P. Natl. Acad. Sci. USA, 108, E1099–E1099, doi:10.1073/pnas.1114634108, 2011. 20077, 20090

Remer, L. A., Kaufman, Y. J., Mattoo, S., Martins, J. V., Ichoku, C., Levy, R. C., Kleidman, R. G., Tanré, D., Chu, D. A., Li, R. R., Eck, T. F., Vermote, E., and Holben, B. N.: The MODIS algorithm, products and validation, J. Atmos. Sci., 62, 947–973, doi:10.1175/JAS3385.1, 2005. 20090

Schulz, M., Textor, C., Kinne, S., Balkanski, Y., Bauer, S., Berntsen, T., Berglen, T., Boucher, O., Dentener, F., Guibert, S., Isaksen, I. S. A., Iversen, T., Koch, D., Kirkevåg, A., Liu, X., Montanaro, V., Myhre, G., Penner, J. E., Pitari, G., Reddy, S., Seland, Ø., Stier, P., and Takemura, T.: Radiative forcing by aerosols as derived from the AeroCom present-day and pre-industrial simulations, Atmos. Chem. Phys., 6, 5225–5246, doi:10.5194/acp-6-5225-2006, 2006. 20076, 20083, 20088, 20103

Smirnov, A., Holben, B. N., Eck, T. F., Dubovik, O., and Slutsker, I.: Effect of wind speed on columnar aerosol optical properties at Midway Island, J. Geophys. Res., 108, 4802, doi:10.1029/2003JD003879, 2003. 20081

ACPD
12, 20073–20111, 2012

Stevens, B. and Feingold, G.: Untangling aerosol effects on clouds and precipitation in a buffered system, Nature, 461, 607–613, doi:10.1038/nature08281, 2009. 20075

Wielicki, B. A., Barkstrom, B. R., Harrison, E. F., Lee, R. B., Smith, G. L., and Cooper, J. E.: Clouds and the Earth's Radiant Energy System (CERES): an Earth observing system experiment, B. Am. Meteorl. Soc., 77, 853–868, 1996. 20090

Yu, H., Dickinson, R. E., Chin, M., Kaufman, Y. J., Zhou, M., Zhou, L., Tian, Y., Dubovik, O., and Holben, B. N.: Direct radiative effect of aerosols as determined from a combination of MODIS retrievals and GOCART simulations, J. Geophys. Res., 109, D03206, doi:10.1029/2003JD003914, 2004. 20076

Yu, H., Kaufman, Y. J., Chin, M., Feingold, G., Remer, L. A., Anderson, T. L., Balkanski, Y., Bellouin, N., Boucher, O., Christopher, S., DeCola, P., Kahn, R., Koch, D., Loeb, N., Reddy, M. S., Schulz, M., Takemura, T., and Zhou, M.: A review of measurement-based assessments of the aerosol direct radiative effect and forcing, Atmos. Chem. Phys., 6, 613–666, doi:10.5194/acp-6-613-2006, 2006. 20076, 20082, 20083, 20085, 20086, 20103

ACPD

12, 20073–20111, 2012

Table 1. Parameters used to derive the anthropogenic aerosol optical depth over land and to prescribe aerosol optical properties for the four aerosol components. The single-scattering albedo is given at 0.55 µm. Optical properties for the anthropogenic aerosol component are prescribed regionally. Representative AERONET sites refer to the sites studied by Dubovik et al. (2002). For the other components, optical properties are prescribed globally.

Aerosol type	Regional boundaries		Anthropogenic fraction over land	Representative AERONET site	Single-scattering albedo
Mineral dust				Cape Verde	0.98
Sea-salt				Hawaii	0.99
Fine-mode natural					0.98
Anthropogenic:					
North America	90° N–30° N	180° W–30° W	0.69	GSFC (USA)	0.98
Eurasia	90° N–30° N	30° W–180° E	0.77	Créteil (France)	0.94
Central America	30° N–0	120° W–60° W	0.63	Mexico City (Mexico)	0.90
South America	30° N–90° S	180° W–30° W	0.69	Brazil	0.91
Africa and Oceania	30° N–90° S	30° W–180° E	0.77	Mongu (Zambia)	0.86
India	30° E–120° E	30° N–10° S	0.82	Maldives	0.91

ACPD
12, 20073–20111, 2012

Table 2. Total and component aerosol optical depths (AOD), direct radiative effects (DRE), and direct radiative effect efficiencies (DREE), for the MACC re-analysis over the period 2003–2010, in global, ocean, and land averages. Optical depths are given at 0.55 µm. Direct effects, in Wm^{-2}, and efficiencies, in Wm^{-2} per unit AOD, are for the shortwave spectrum and cloud-free conditions, and given at the top of atmosphere (TOA), surface, and within the atmosphere. See text for calculation of uncertainties.

		TOA		Surface		Atmosphere
Aerosol type	AOD	DRE	DREE	DRE	DREE	DRE
			Global			
Total	0.180 ± 0.040	−7.6 ± 4.2	−42	−10.2 ± 5.5	−57	+2.6
Anthropogenic	0.048 ± 0.019	−1.8 ± 1.0	−38	−3.9 ± 2.1	−81	+2.1
Mineral dust	0.043 ± 0.017	−1.4 ± 0.8	−33	−1.9 ± 1.0	−44	+0.5
Sea-salt	0.080 ± 0.031	−4.0 ± 2.2	−50	−4.1 ± 2.2	−51	+0.1
Fine-mode natural	0.009 ± 0.004	−0.3 ± 0.2	−33	−0.3 ± 0.2	−33	+0.0
			Ocean			
Total	0.170 ± 0.036	−8.0 ± 3.1	−47	−9.6 ± 4.4	−56	+1.6
Anthropogenic	0.028 ± 0.009	−1.3 ± 0.5	−46	−2.6 ± 1.2	−93	+1.3
Mineral dust	0.030 ± 0.009	−1.0 ± 0.4	−33	−1.3 ± 0.6	−43	+0.3
Sea-salt	0.112 ± 0.035	−5.7 ± 2.2	−51	−5.8 ± 2.7	−52	+0.1
Fine-mode natural			N/A			
			Land			
Total	0.203 ± 0.047	−6.4 ± 4.3	−32	−11.5 ± 6.6	−57	+5.1
Anthropogenic	0.098 ± 0.039	−3.1 ± 2.1	−32	−7.0 ± 4.0	−71	+3.9
Mineral dust	0.074 ± 0.030	−2.4 ± 2.3	−32	−3.3 ± 1.9	−45	+0.9
Sea-salt			N/A			
Fine-mode natural	0.032 ± 0.013	−0.9 ± 0.6	−28	−1.1 ± 0.6	−34	+0.2

ACPD
12, 20073–20111, 2012

Table 3. Summary of uncertainty analysis on globally-averaged anthropogenic aerosol optical depth (AOD) at 0.55 µm, anthropogenic direct radiative effect (DRE, Wm^{-2}) at top-of-atmosphere, and direct radiative forcing (DRF, Wm^{-2}) at top-of-atmosphere. Period is 2003–2010. See text for details.

Quantity	Best estimate	Uncertainty	Source for uncertainty
Anthropogenic AOD	0.048	Due to total AOD retrieval: ±0.011 (22 %) Due to algorithm: ±0.007 (15 %) *Overall*: ±0.018 (37 %)	Yu et al. (2006) Bellouin et al. (2005)
Cloud-free anthr. DRE	−1.8	Due to anthropogenic AOD: ±0.7 Due to optical properties: ±0.3 *Overall*: ±1.0 Wm^{-2} (55 %)	From above and DREE in Table 2 Bellouin et al. (2005)
Cloud-free DRF All-sky DRF	−1.6 −0.5	*Overall*: ±0.9 (55 %) From cloud-free: ±0.3 From cloudy-sky: +0.1 ± 0.1 *Overall*: −0.4 ±0.4 Wm^{-2}	Same as anthropogenic DRE Cloud-free DRF scaled by cloud-free fraction Schulz et al. (2006); Bellouin et al. (2008)

ACPD
12, 20073–20111, 2012

Table 4. Anthropogenic aerosol direct radiative forcing (DRF) in cloud-free and all-sky conditions, and first indirect radiative forcing (IRF) and total aerosol radiative forcing (RF) in all-sky conditions, as derived from the MACC re-analysis over 2003–2010. All values are in Wm^{-2} at the top of the atmosphere (TOA), unless where stated, for the shortwave spectrum only. See text for calculations of uncertainties and upper and lower bounds, which have been assessed for global values only in all-sky.

	Global	Ocean	Land
Cloud-free DRF	−1.6 ± 0.9	−1.3 ± 0.5	−2.5 ± 1.7
Cloud-free DRF (surface)	−3.6 ± 1.9	−2.5 ± 1.1	−6.5 ± 3.7
All-sky DRF	−0.5 [−0.8 to 0.0]	−0.4	−0.8
All-sky IRF	−0.4 [−2.1 to −0.1]	−0.4	−0.2
All-sky RF	−0.9 [−2.9 to −0.1]	−0.8	−1.2

ACPD
12, 20073–20111, 2012

Table 5. Uncertainty analysis for the first aerosol indirect forcing. All values are in Wm^{-2}.

Best estimate	Uncertainty range for albedo sensitivity	Uncertainty range for droplet number sensitivity	Uncertainty range for anthropogenic AOD	Total uncertainty range
−0.4	−0.5 to −0.3	−1.4 to −0.2	−0.4 to −0.2	−2.1 to −0.1

ACPD
12, 20073–20111, 2012

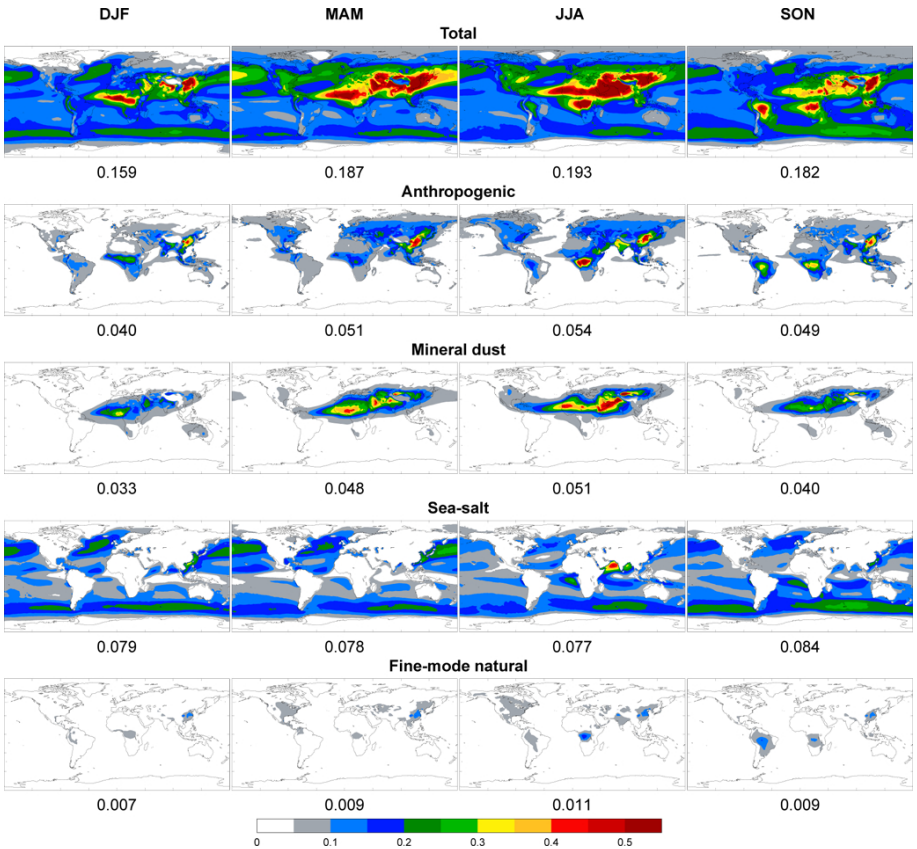

Fig. 1. Seasonal distributions of aerosol optical depth at 0.55 µm as derived from the MACC re-analysis over 2003–2010. From top to bottom, the optical depth is for total, anthropogenic, mineral dust, sea-salt, and fine-mode natural aerosols. Global averages are given by the numbers below each panel.

ACPD
12, 20073–20111, 2012

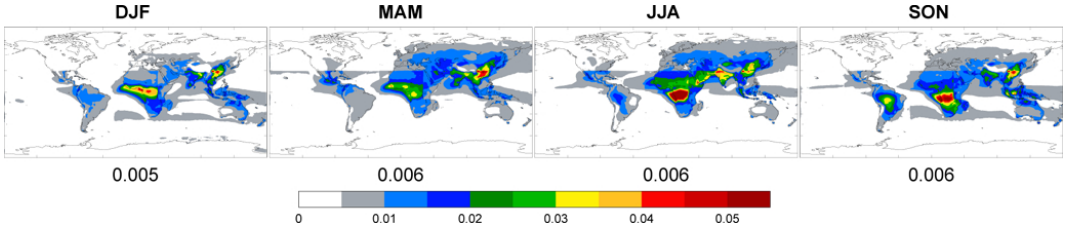

Fig. 2. Seasonal distributions of total absorption AOD at 0.55 µm as derived from the MACC re-analysis over 2003–2010. Global averages are given by the numbers below each panel.

ACPD
12, 20073–20111, 2012

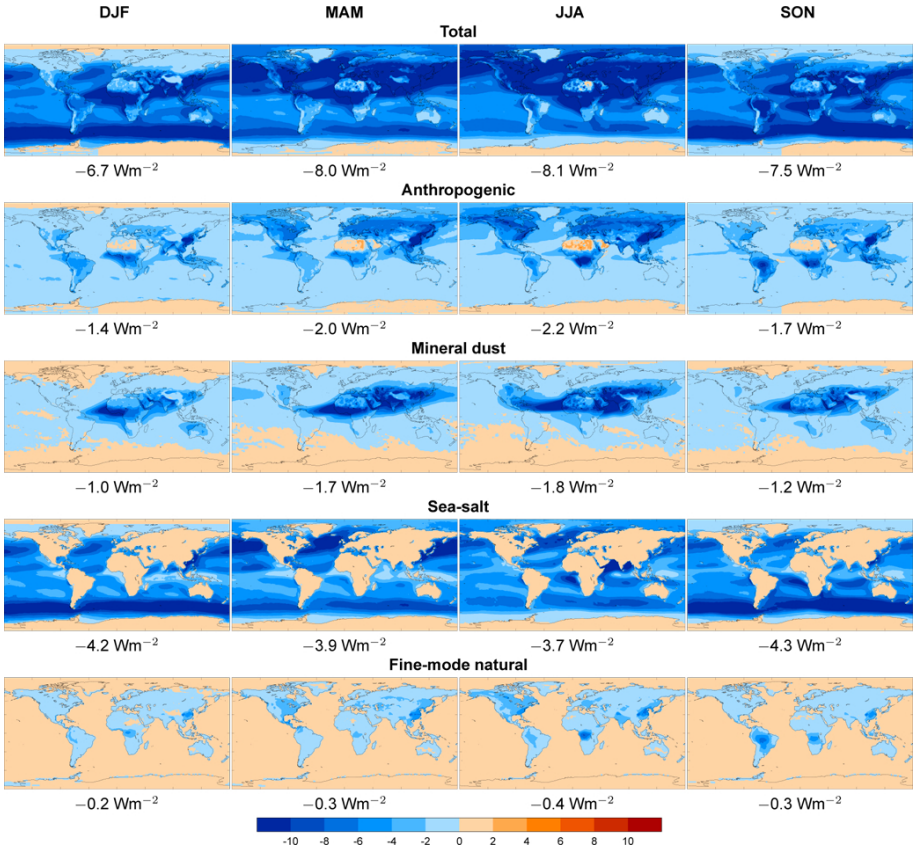

Fig. 3. Seasonal distributions of shortwave direct radiative effect in cloud-free sky at the top of the atmosphere, in Wm^{-2}, as derived from the MACC re-analysis over 2003–2010. From top to bottom, the direct effect is for total, anthropogenic, mineral dust, sea-salt, and fine-mode natural aerosols. Global averages are given by the numbers below each panel.

ACPD
12, 20073–20111, 2012

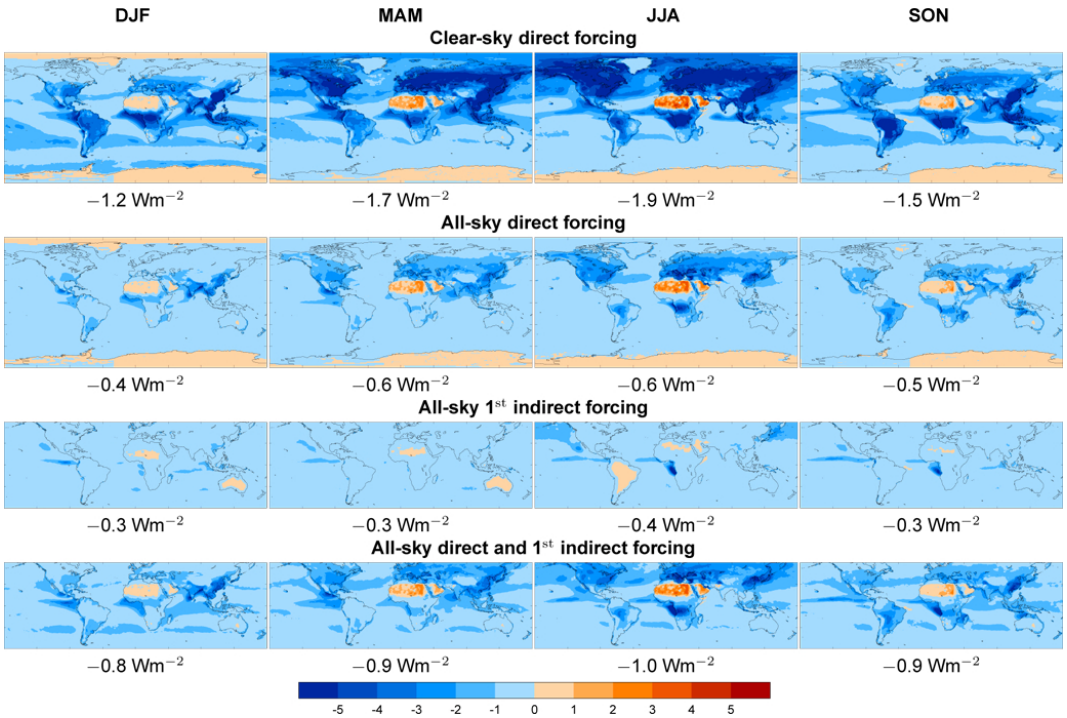

Fig. 4. Seasonal distributions of shortwave aerosol forcing at the top of the atmosphere, in Wm^{-2}, as derived from the MACC re-analysis over 2003–2010. From top to bottom, clear-sky (or cloud-free) direct forcing, all-sky direct forcing, all-sky first indirect forcing, and the sum of all-sky direct and first indirect forcing. First indirect forcing is not estimated poleward of 60° latitude. Global averages are given by the numbers below each panel.

ACPD
12, 20073–20111, 2012

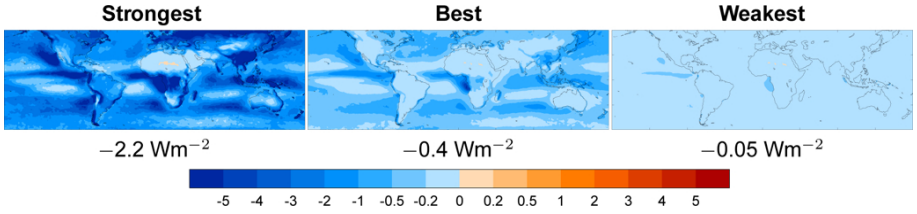

Fig. 5. Multi-annual averaged distributions of strongest, best, and weakest estimates of shortwave all-sky first indirect forcing at the top of the atmosphere, in Wm^{-2}. Global averages are given by the numbers below each panel.

ACPD
12, 20073–20111, 2012

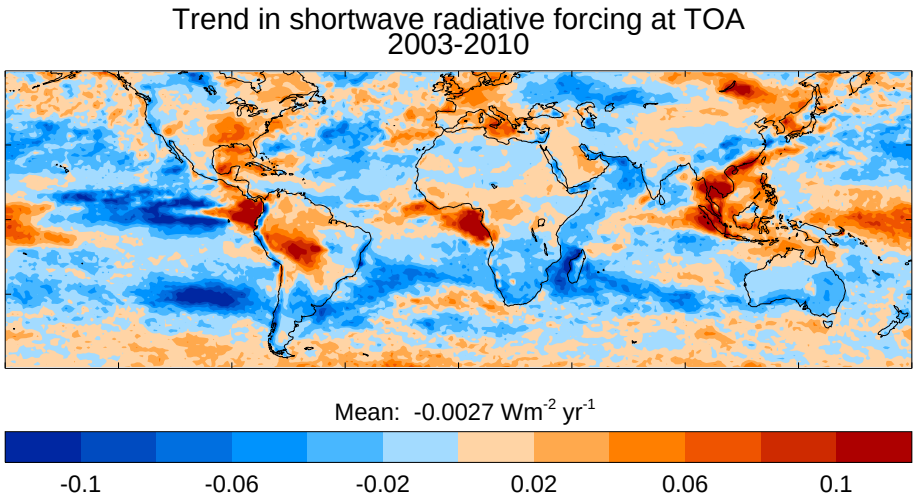

Fig. 6. Trend in aerosol radiative forcing, in $Wm^{-2}yr^{-1}$, as derived from the MACC aerosol re-analysis for 2003–2010. Negative numbers correspond to a strengthening of the aerosol radiative forcing.

ACPD
12, 20073–20111, 2012